Master's Thesis

EXPERIMENTAL STUDY OF CORROSION ON STRUCTURAL MATERIALS FOR PYROCHEMICAL PROCESS IN HIGH TEMPERATURE MOLTEN SALTS CONTAINING FISSION PRODUCTS

Hyeonjun Jeong

Department of Nuclear Engineering

Graduate School of UNIST

2019

EXPERIMENTAL STUDY OF CORROSION ON STRUCTURAL MATERIALS FOR PYROCHEMICAL PROCESS IN HIGH TEMPERATURE MOLTEN SALTS CONTAINING FISSION PRODUCTS

Hyeonjun Jeong

Department of Nuclear Engineering

Graduate School of UNIST

EXPERIMENTAL STUDY OF CORROSION ON STRUCTURAL MATERIALS FOR PYROCHEMICAL PROCESS IN HIGH TEMPERATURE MOLTEN SALTS CONTAINING FISSION PRODUCTS

A thesis
submitted to the Graduate School of UNIST
in partial fulfillment of the
requirements for the degree of
Master of Science

Hyeonjun Jeong

Jan 9, 2019
Approved by

_____

Advisor
Hee Reyoung Kim

EXPERIMENTAL STUDY OF CORROSION ON STRUCTURAL MATERIALS FOR PYROCHEMICAL PROCESS IN HIGH TEMPERATURE MOLTEN SALTS CONTAINING FISSION PRODUCTS

Hyeonjun Jeong

This certifies that the thesis of Hyeonjun Jeong is approved.

Jan 9, 2019

signature

_____

Advisor: Hee Reyoung Kim

signature

_____

Jaeyeong Park: Thesis Committee Member #1

signature

_____

Sungyeol Choi: Thesis Committee Member #2

Abstract

In the real pyroprocessing operating environment, fission products such as rare earth, lanthanide and TRU are dissolved into electrolyte as impurities. With increasing number of batches, corrosion time and the concentration of impurities also increase, but there is a lack of research to study the effect on corrosion behavior. When LiCl-KCl electrolyte are recovered, new electrolyte would affect the corrosion behavior of structural material in initial period, but most corrosion studies just perform one-time measurement of properties for selected corrosion period, so initial timely corrosion behavior is not clearly explained. This study concentrates on revealing the effect of impurities on corrosion behavior, and research initial corrosion behavior by timely measurement with electrochemical techniques. Tested YCl_3 as a representative rare earth impurity dissolved in LiCl-KCl eutectic salt to assess the effect of fission product impurities on corrosion behavior. With electrochemical techniques, verified the reliability of electrochemical cell and measured corrosion rate of Inconel 600. For precise observation of initial corrosion behavior, hourly measured electrochemical properties for 100 hours. Observed the corrosion behavior on intensive conditions to overcome the restriction of 100 hours by testing some cases on 873K.

CONTENTS

I. Introduction

1.1 General Backgrounds

The efficient management of spent nuclear fuel is one of major issues in nuclear fuel cycle. From the first operation of commercial nuclear power plant in 1956, considerable amount of spent nuclear fuels had been created worldwide by nuclear power plants which were managed with various methods for disposal or recycling of the spent nuclear fuels. Generally spent nuclear fuels discharged from commercial Light Water Reactors (LWRs) contain high activity fission products such as ^{90}Sr and ^{137}Cs emitting considerable heat for hundreds of years and long lived fission products (actinides, actinides daughters; ^{99}Tc, ^{129}I and ^{79}Se) for a few hundred thousand years, which is closely related with the cost of storage and disposal. **Fig 1.** shows the relative activity of discharged fuel components categorized by decay time [1]. After the cooling and storage process of spent nuclear fuels in AR pool and interim storage facilities, the radioactive wastes are moved to disposal process. Since the criteria of deep geological disposal are generally set considering the radioactivity of mined uranium ore (barely radioactive) to avoid potential health hazard from inhalation, the site and design of disposal facility are determined to isolate spent nuclear fuels for hundreds of thousands years, and the cost of disposal increase with the volume of radioactive wastes.

Major NEA countries generally take one or both of spent fuel management strategies: reprocessing and direct disposal [2]. **Table 1** shows that France and Japan reprocesses spent fuels to recycle them as MOX fuel. However, Finland and Sweden chose direct disposal, US stopped reprocessing in 1977 and also decided to manage spent fuels by direct disposal. Despite of many advantages, reprocessing, especially conventional aqueous reprocessing has been criticized with bad economic efficiency and risk of nuclear proliferation. In South Korea, there have been no definitive policies for long term used fuel management and the both strategies are still under consideration. However, the necessity for establishing management direction and making social consensus is getting magnified since accumulation status of spent nuclear fuel is reaching to allowed capacity near future. **Table 2** shows the status of accumulated spent nuclear fuel on each reactor site [3]. The saturation of Wolsong, Kori, Hanbit and Hanul site is estimated within 10 years, especially Wolsong in 2021. The tentative direction of high level waste (HLW) management is direct disposal [2], but dry reprocessing technology is also considered as an alternative and collaborative research projects on pyroprocessing are in progress between South Korea and US. Pyroprocessing is considered that it has better proliferation-resistance than aqueous reprocess, and the potential cost savings of spent nuclear management by the separation of spent nuclear fuel compositions.

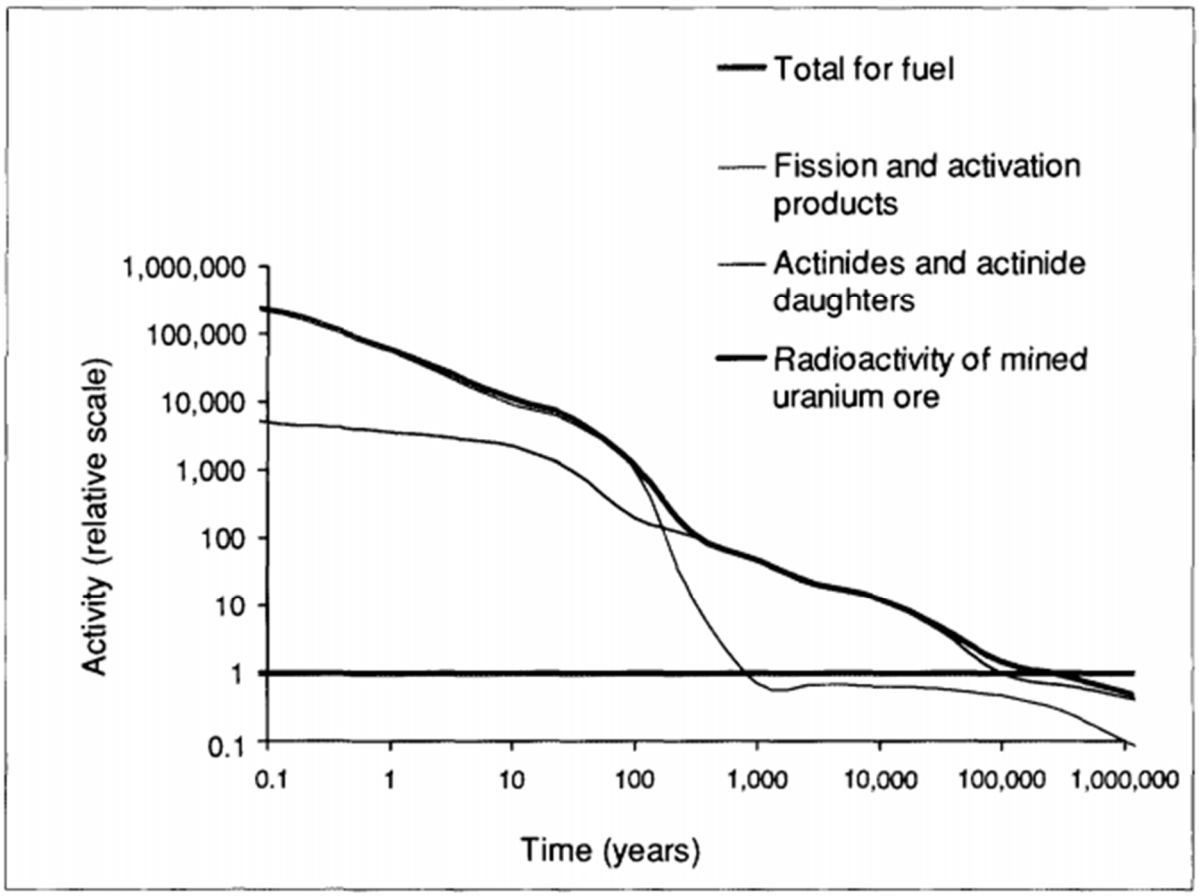

Fig. 1. The decaying time of high activity and long lived fission products

Table 1. Spent nuclear fuel management strategies in OECD/NEA countries

Country	Type (Spent fuel)			
Australia	RR	- reprocessing abroad - returning to supplier (US)	Weight unit; N assemblies	Storage on-site (Lucas Heights).
Austria	RR	- returning to supplier (US)	Weight unit; N assemblies	Not planned.
Belgium	NPP/RR	- reprocessing (earlier) - no strategy (direct disposal considered currently)	Weight unit; N assemblies	On-site storage; Central storage (Dessel HLW); DGR – advanced concept.
Canada	NPP/RR	- direct disposal as HLW	Weight unit; N assemblies	Long-term dry storage at each reactor site. Common storage facility at each multi-reactor site (four to eight reactors served by single storage facility); DGR – in siting.
Czech Republic	NPP/RR	- direct disposal - reprocessing (under consideration)	Weight unit; N assemblies	Central storage – Dukovany; DGR – early siting.
Denmark	RR	- storage - disposal abroad (if possible)	Weight unit	No planned.
Finland	NPP/RR	- direct disposal	Weight unit; N assemblies	On-site storage; DGR – Olkiluoto (construction licence granted).
France	NPP/RR	- reprocessing	Weight unit	Storage on-site; Central storage (La Hague); DGR – CIGEO (underground research laboratory stage).
Germany	NPP/RR	- reprocessing (stopped in 2005) - direct disposal/ returning to supplier	Weight unit	Central + on-site storage (Ahaus + Gorleben); DGR – siting (restarted).
Greece	RR	- returning to supplier - interim storage	Weight unit; N assemblies	No planned.
Hungary	NPP/RR	- no strategy on disposal - long-term storage	N assemblies	Central storage DGR – early siting – ISFSF; .
Iceland	-	-	-	-
Ireland	-	-	-	-
Italy	NPP/RR	- reprocessing abroad (in France)	Weight unit; N assemblies	In site and outside storages – (including Elk River U-Th SF).
Japan	NPP/RR	- reprocessing (can be revised)	Weight unit	On-site storage; Central storage – Mitsu; DGR – siting.

Table 1. Spent nuclear fuel management strategies in OECD/NEA countries (cont'd)

Korea	NPP/RR	- direct disposal (can be revised, not finally decided).	Weight unit;	On-site pool storage; Central storage – planned; DGR – early siting.
Luxembourg	-	-	-	-
Mexico	NPP	- no strategy.	Weight unit;	On-site pool storage; DGR – concept in general.
Netherlands	NPP/RR	- reprocessing abroad (France); - RR – disposal as HLW.	Weight unit; N assemblies	Storage (COVRA); DGR – concept in general.
Norway	RR	- disposal; - reprocessing abroad	Weight unit;	Storage (IFE); DGR –concept in general.
Poland	RR	- returning to supplier; - no strategy for future management	Weight unit; N assemblies	DGR – siting (start).
Portugal	RR	- returning to supplier	Weight unit; N assemblies	No planned.
Russia	NPP/RR	- reprocessing; - direct disposal (possible for some types).	Weight unit; N assemblies	On-site storage dry and wet; Central storage – Mountain Mining Combine (MCC); DGR – Underground Research Laboratory designing stage.
Slovak Republic	NPP/RR	- - direct disposal; reprocessing abroad	Weight unit; N assemblies	On Central storage; -site storage; DGR – concept in general.
Slovenia	NPP	- direct disposal or; - reprocessing abroad or; - multinational approach.	N assemblies	On-site wet storage; DGR – early stage.
Spain	NPP/RR	- reprocessing up to 1983; - direct disposal.	Weight unit; N assemblies	Central storage – ATC; DGR – research.
Sweden	NPP/RR	- direct disposal.	Weight unit; N assemblies	Central storage – CLAB; DGR – Forsmark (Osthammar).
Switzerland	NPP/RR	- reprocessing; - not reprocessed SF as HLW.	Weight unit; N assemblies	On-site storage; Central storage – Zentrales Zwischenlager (ZZL); DGR – siting.
Turkey*	RR	- reprocessing (as option – TBD); - direct disposal (as option – TBD).	Weight unit;	DGR.
United Kingdom	NPP/RR	- - reprocessing; direct disposal under consideration	Weight unit;	Storage DGR – early siting (50 years). – Sellafield;
United States	NPP/RR	- reprocessing up to 1977; - direct disposal as HLW (can be revised).	Weight unit;	On-site storage wet and dry; DGR – (Yucca Mountain), implementation is suspended.

Table 2. Status of spent nuclear fuel storage by reactor type and site (Jun. 2018)

	PHWR	**PWR**				
	Wolsong	*Kori*	*Hanbit*	*Hanul*	*Shin Wolsong*	*Saeul*
Saturation Percentage (%)	88.3	77.7	67.7	77.4	36.9	12.8
Capacity (Bundle)	499,632	7,994	9,017	7,066	1,046	780
Accumulation (Bundle)	441,320	6,215	6,103	5,466	386	100
Expected Saturation (Year)	2021	2028	2024	2026	2038	-

1.2 Pyroprocessing flowsheet

In Korea, reprocessing is on developing to be a part of combined spent nuclear fuel management system connecting pyroprocessing with Sodium-cooled fast reactor (SFR). Oxide spent nuclear fuels discharged from PWR reactor are reduced within pyroprocessing to metallic fuels containing TRU waste which used in SFR. The standard spent nuclear fuel is created from the 10MTHM oxide fuels of which the initial U-235 enrichment is 4.5wt%, at a burnup of 45GW-d/t U, cooled at least 5 years. Pyroprocessing is an integrated technique of 7 subprocess; (1) fuel-element chopping and decladding (2) high temperature voloxidation (3) electrolytic reduction (4) Electrorefining (5) Electrowinning (6) Salt purification and (7) fuel fabrication. **Fig. 2** shows the summary of pyroprocessing flowsheet.

In chopping/decladding process, 99% or more recovery ratio of fuel materials is required from spent nuclear fuel rod to minimize the loss of materials. In DUPIC system, about 99.99% of spent fuel materials are recovered. By adopting oxidative decladding technique, the fuels are detached from cladding in powder form by non-stoichiometry chemical expansion. In this subprocess, the volatile fission gases such as I, Kr and ^{14}C can be released while UO_2 is oxidized to U3O8.

In high temperature voloxidation process, volatile and semi-volatile fission products are reduced from spent fuels. Through an advanced voloxidation process, materials such as I, Cs, Tc, Ru, Te and Mo are removed under the environment of oxygen gas injection, 1250 for 10 hours. **Table 3** shows the removal rate of fission gases on this process [4].

Table 3. Removal rate of fission gases within the voloxidation process

Voloxidation temperature	H-3	C-14	Kr-85	I-129	Cs	Tc	Ru	Rh	Te	Mo
1250	100	100	100	100	98	100	100	80	90	80

In electrolytic reduction process, the spent fuel oxides from PWR reactor reduced to metallic form by electrochemical process. The powder collected from voloxidation process with MgO basket moved to electrochemical cell containing LiCl-3wt% Li_2O electrolyte. Through the electrolytic reduction process, remaining radioactive alkali and alkaline earth metal are dissolved to molten salt electrolyte with chloride forms. Uranium, TRU, rare earth and noble metal oxides are reduced to metallic form at ceramic cathode basket while oxygen gases are produced at anode. The reactions at each electrode are as follows:

Reactions at cathode

$$Li^+ \rightarrow Li + e^-$$

$$M_xO_y + 2yLi \rightarrow xM + yLi_2O$$

Reaction at anode

$$O^{2-} \rightarrow \frac{1}{2}O_2 + 2e^-$$

The reduction and recovery rate of oxides are assumed to be higher than 99.5%. The remaining oxides are collected from metal ingot within electrorefining process, and the dissolved chlorides are collected by electrolytic winning process to be recycled. Cathode consolidation process prevents the loss of molten salt.

In electrorefining process, uranium from the metallic product of electrolytic reduction process is separated and collected at solid cathode while noble elements remain in anode basket. Uranium and small amount of uranium salts deposit on solid cathode, then the salts remaining on cathode are distilled through cathode process to refine the uranium into pure ingot. The electrolyte is composed of LiCl-KCl eutectic salt containing 9wt% of UCl_8, and the concentration of UCl_8 should be enough to prevent the reduction of TRU or RE. During the process, transition metal fission products remain in anode basket since it cannot be oxidized within electrorefining cell condition. The reaction on solid cathode is as follows:

$$UCl_3 + TRU(RE) \rightarrow U + TRU(RE)Cl_3$$

Produced pure uranium partially used on chlorination process to collect RE/TRU oxide dross yielded on cathode process:

$$RE_2O_3 + 2UCl_3 \rightarrow 2RECl_3 + UO + UO_2$$

$$TRU\ O_2 + UCl_3 \rightarrow TRU\ Cl_3 + UO_2$$

The required amount of uranium for chlorination process is proportional to the amount of dross. The RE/TRU chlorides products are moved to the electrowinning process.

In electrowinning process, TRU, U and some impurities are deposited simultaneously by the liquid cadium cathode (LCC) which induces the intermetallic compounds to prevent the separation of pure TRU. The process contains following steps; Separation cadmium from TRU-cadimium intermetallic compound, conversion of product to ingot, diminution of TRU from salt before removing fission products from salts. By the repeated electrorefining process, electrolyte contains accumulated dissolved

RE/TRU chlorides. After the concentration reaches to limit, the electrolyte moved to electrowinning process, then RE/TRU deposit at LCC in proper electrochemical potential range. Since the Gibbs free energy levels to forming chlorides of U, TRUs and part of RE are very similar in LCC, TRU or Plutonium cannot be separated independently. The intermetallic compound of cadmium and RE/U/TRU is separated by cadimium distillation step. Since the melting point of cadmium is lower than TRU, only cadmium is distilled and the remainder are processed to ingot. The recovery rates of TRU and RE are 98.3% and 1.1%, but 100% for uranium. The TRU in salts removed first within drawdown process to processed in electrorefiner again, then the rare earth in salts separated by salt purification process. Consequently, 99.95% of TRU is recovered through the processes.

In salt purification process, the fission products produced from electrolytic reduction and electrowinning process such as Cs, Sr, RE and small amount of TRU are separated from salts. The salts are recycled in pyroprocessing, and fission products are discarded of the ceramic form for Cs and vitrified form for Sr, RE and TRU.

In fuel fabrication process, fuels for SFR are generated using the spent fuels which are converted to U/TRU alloy as the product of pyroprocessing. With the injection casting method, metallic fuel rods containing TRU are fabricated by adding uranium ingot from pyroprocessing, Zr. The fuel composition, U:TRU:Zr is assumed to 65:20:10 and less than 5% for RE.

The total waste expept for metal waste generated from pyroprocessing adopted for 10MTHM of spent fuel from PWR using 4.5wt% of ^{235}U, 45000MWd/MT U and 5 years cooling is about 1610kg, and it is about 16wt% of initial fuel weight. High level waste is 812kg, and it is about 8.1wt% of initial fuel weight. **Table 4** shows the summary of total waste.

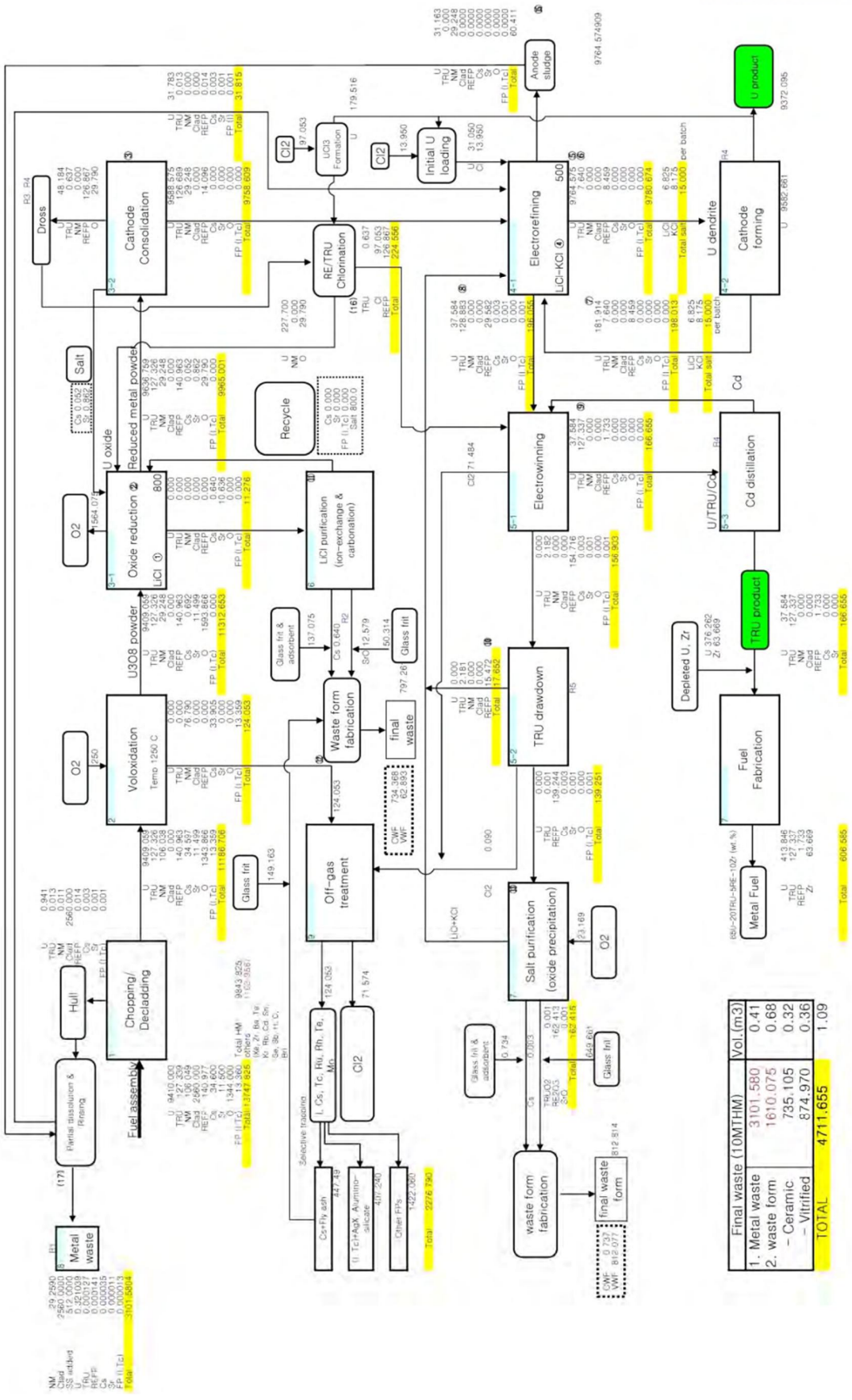

Fig 2. The flowsheet of pyroprocessing with material tracking for each subprocesses

Table 4. Summary of radioactive waste from pyroprocessing by characteristics

Waste form / Characteristic	LLW			HLW
	Metal	Ceramic	Vitrified[1)]	Vitrified[2)]
Weight [kg]	3100	735	63	812
Volume [m3]	0.41	0.32	0.03	0.33
Decay heat [W/m3]	9.08×10^{-2}	1.97×10^{4}	3.63×10^{4}	7.78×10^{4}
α-activity [Bq/g]	1.53×10^{4}	0	0	4.58×10^{5}

1) Waste LiCl salt are included in Sr

2) Waste LiCl-KCl salt are included in RE and TRU

1.3 Mechanism of Corrosion in Molten Chloride Salts

Corrosion is the loss of metallic materials occurring on surface of metals to forming electrochemically more stable compounds. The outer materials surrounding metals involved in the corrosion reactions can be gases or liquids affecting the corrosion behavior of metals by the interaction with the components of alloys. The products of corrosion are generally oxides adhering on metal surface protecting further corrosion as passivation layers or salts dissolved in the outer materials. However, in case of corrosions in molten chloride salts environment blocking the inflow of oxygen, the oxide layers are not formed, but the existing oxide layers can contribute to the corrosion resistance of metallic alloys.

The structural materials of the pyroprocessing electrochemical cells should have strong corrosion resistance to endure the corrosive molten salt environment. Through the entire process, LiCl-KCl eutectic salt is the key medium for electrorefining and electrowinning at the temperature of about 500 . During each batch of processes, various fission products from spent fuels such as RE and TRU are dissolved to the salt as impurities, so the concentration of impurities may not be fixed in actual operation. For chloride salts, intrinsic corrosion is hard to occurs because the thermodynamic stability of salt components are more stable than metal salts from structural materials [5].

The lower the Gibbs free energy, the easier it is to form and the more stable it is. In the LiCl-KCl molten salt environment, the corrosion mechanism can be predicted by comparing the formation Gibbs free energy of chloride. For a more accurate analysis, the activity of the constituents should also be determined and analyzed through the Nernst equation to predict equilibrium potential and expected reactions. **Table 5** shows standard Gibbs free energies for selected materials at 773K and 873K [6-7]. Since YCl3 is less stable than LiCl or KCl, chloride ion exchange between metal and yttrium ions occurs prior than LiCl or KCl ions. The effect of YCl3 on corrosion would increase continuously with increasing batches and concentration of YCl3, according to Nernst equation. The difference between Gibbs free energy of each components of Inconel 600 would induce selective leaching.

Table 5. Standard Gibb's free energy of selected materials at 773K and 873K

	773K (KJ/mol Cl_2)	873K (KJ/mol Cl_2)
$CrCl_3$	-60.4	-57
$FeCl_2$	-58.8	-55.2
$NiCl_2$	-45.7	-42.5
LiCl	-165.1	-161.4
KCl	-172	-167.5
YCl_3	-130.2	-124.9

II. Literature Review

2.1 Super alloys utilized in molten chloride eutectic salts

Molten chloride salts are used for wide range of temperatures for various purposes. Since the range of temperature can determine the range of utilization, low melting temperature and high boiling temperature is sometimes the indicators of usefulness, but achieve both advantages is hardly available with a single chloride salt. An good solution for this problem is the mixture of different chloride salts to make eutectic salts, which can possess both advantages from two or more of the component salts. However, this yields new problem on corrosion issues, since there is possibility that the mixture of chloride salts can accelerate corrosion of alloys used on the chloride salts environment. There are some studies on corrosion behavior in binary eutectic salts environment, but studies on ternary eutectic salts systems are not enough [8].

There are several types of candidate alloys studied for utilization in molten chloride mixture salts. For NaCl-KCl-$ZnCl_2$, Hastelloys super alloys such as C-276, C-22 and N types were tested at 773K. Among these Hastelloy alloys, C-276 shows highest corrosion resistance with the penetration rate of 0.04 mm/yr [9]. M. Hoifmeister et. al. tested stainless steel with different carbon concentration and Ni-based super alloys in LiCl-KCl-CsCl eutectic salt environment. For stainless steels, low carbon concentration alloys have advantages on preventing passivation layers and shows relatively low corrosion rate. The corrosion resistance of Ni-based super alloy were best; even at as high as 800K temperature CMSX-4 alloys shows low corrosion rate [10]. A. Ravi Shankar et. al. tested low Cr and high Cr steels and three Ni-based alloys in LiCl-KCl environment at 873K under Argon atmosphere. **Fig. 3** shows the intrinsic corrosion test results of candidate materials with time for hundreds hours. Steel alloys shows high percentage of weight loss, but Ni-based alloy get weight by corrosion test when hundreds hours passed. There were adherent corrosion products on the surface of Ni-based alloys. SEM-EDAX micrographs of Ni-based alloys shows that there are Cr-Fe rich corrosion products region with porous matrix and faceted grains. Shankar guessed that the weight gain is due to the growth of Fe-rich particles on surfaces, but it caused by other specimens simultaneously tested in the same cell. If there is just a Ni-based alloy for test crucible, the weight of alloy would decrease at the end of experiment [11].

2.2 Effect of alloying elements on corrosion resistance

With the presence of chloride, even small amount of oxygen or water can cause reactions with chlorides to forming oxychloride, hydrochloric acid and chlorine gas. Although the inflow of oxygen or moisture is well blocked, oxide layer or ceramics containing oxygen react with chloride and would form corrosion products with materials constitute alloys.

J.I.Barraza-Fierro et. al. suggested corrosion mechanism of oxide layer formation with the presence of oxygen ion and moisture. At the initial phase of corrosion, metal chlorides are formed and dissolved LiCl-KCl eutectic salt with gaseous form. If there are oxygen ion in LiCl-KCl eutectic salt, metal chloride gases react with it and forms Metal oxide as a corrosion product. If an element of the alloy has lower free energy than other, the element forms corrosion products at outer zone and the other element forms at inner zone. **Fig. 4** shows the sequence of oxides formation [12]. The solubility of oxygen ion or moisture is closely related with the concentration at atmosphere. These impurities should be excluded to measure corrosion behavior of specimens to replicate normal operation environment of electrorefining process. Also, the oxide layer adhered on the surface of specimen should be detached by dedicated polishing.

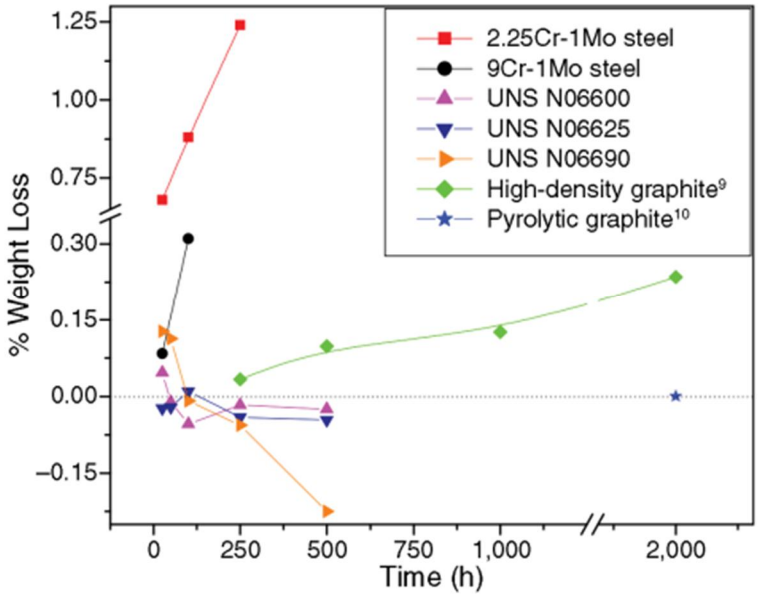

Fig. 3. Weight loss (%) of 2 stainless steels and 3 Ni-based super alloys up to 500 h, 2 graphite materials for up to 2000 h.

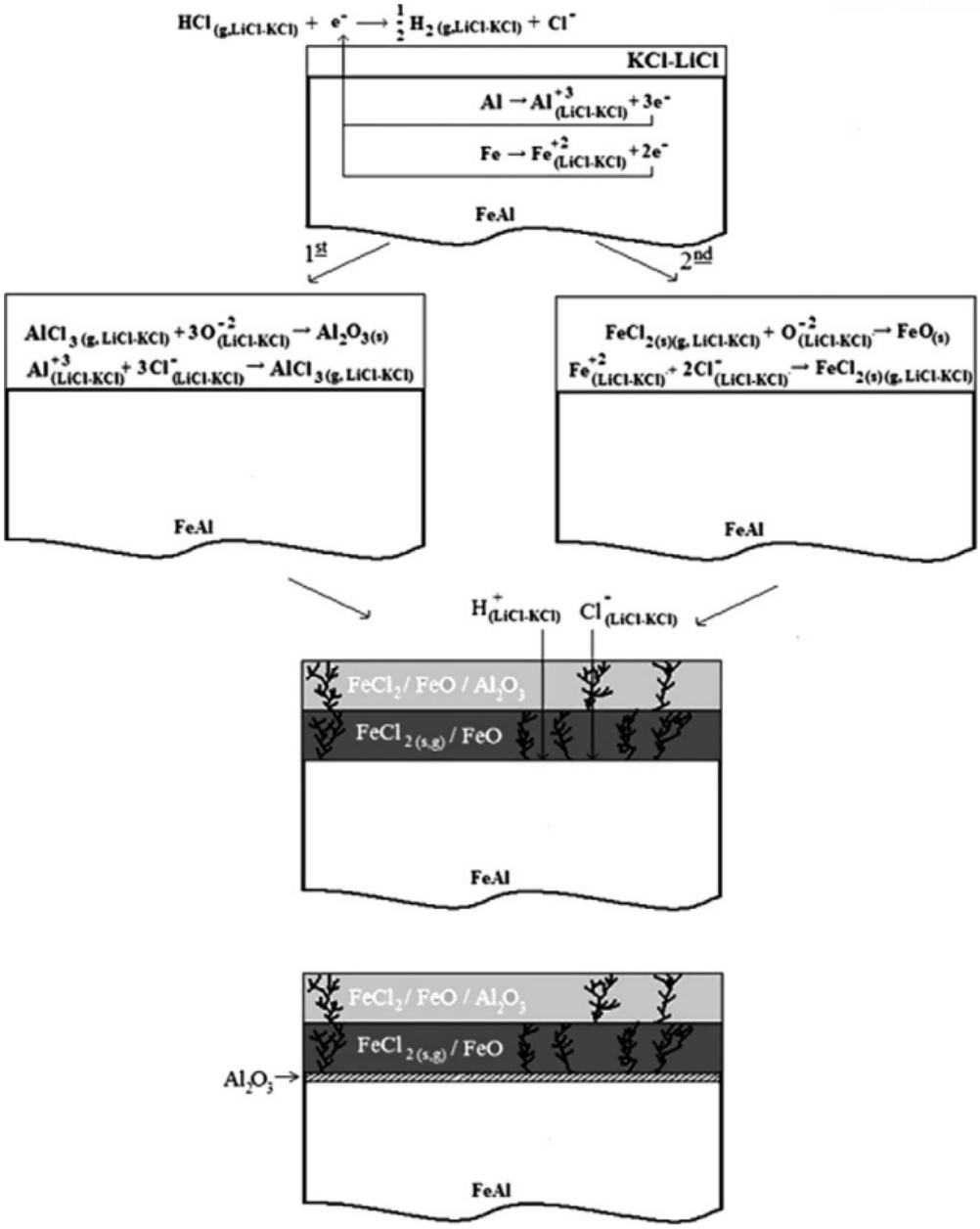

Fig. 4. Mechanism of separated oxide layer formation for Fe-40at% Al intermetallic alloy.

III. Research Objective and Scope

3.1 Research Objective

In the real pyroprocessing operating environment, fission products such as rare earth, lanthanide and TRU are dissolved into electrolyte as impurities. With increasing number of batches, corrosion time and the concentration of impurities also increase, but there is a lack of research to study the effect on corrosion behavior. When LiCl-KCl electrolyte are recovered, new electrolyte would affect the corrosion behavior of structural material in initial period, but most corrosion studies just perform one-time measurement of properties for selected corrosion period, so initial timely corrosion behavior is not clearly explained. This study concentrates on revealing the effect of impurities on corrosion behavior, and research initial corrosion behavior by timely measurement with electrochemical techniques.

3.2 Research Scope

i. Test YCl_3 as a representative rare earth impurity dissolved in LiCl-KCl eutectic salt to assess the effect of fission product impurities on corrosion behavior.

ii. Concentrate on Ni-based alloy to carefully analyze the effect of impurities.

iii. For precise observation of initial corrosion behavior, hourly measure electrochemical properties for 100 hours.

iv. Observe the corrosion behavior on intensive conditions to overcome the restriction of 100 hours by testing some cases on 873K

IV. Electrochemical Measurement

4.1 Experimental Methods

4.1.1 Specimen preparation

Nickel based alloy Inconel 600 were used to experimental samples. **Table 6** shows general as-received composition of the tested material. The sample metal plates were cut to the sample size of W6*D3*H40 with a hole for connection with tungsten wire. Fig. 1 shows the shape and schematic diagram of sample specimens. Each face of specimens was sequentially polished using 320-400-600-800-grit SiC paper, by changing rubbing direction for each polishing steps by 90°, then abraded by 6-3-1 μm grinding powder step by step with lubricant. After that, the specimens were cleaned by detergent and distilled water manually, dried by air gun, then kept in glove box of argon atmosphere. During corrosion experiment the samples were hang by Tungsten or Molybdenum hook wire with the small hole made at upper side and put in the cell carefully to prevent the shortcut with other electrodes. After all of the electrochemical measurement are finished, specimens are pulled out from the cell and cooled for 1 hours. The area of working electrode contacting with the electrolyte were measured by the height of remaining salt, then cleaned with distilled water and acetone using ultrasonic cleaner.

Table 6. Chemical composition of samples

Material	*C*	*Cr*	*Fe*	*Mn*	*Mo*	*Ni*	*P*	*S*	*Si*
Inconel 600	≤0.08	14-17	6-10	1	-	≥72	-	0.002	≤0.5

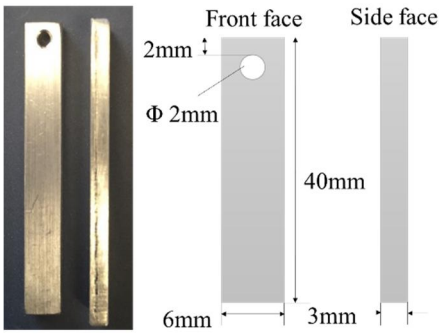

Fig. 5. Picture and shape of specimen for corrosion test. (W6*D3*H40 mm)

4.1.2 Electrolyte preparation with impurities

The actual composition of molten salt electrolyte for pyro processing is not pure LiCl-KCl eutectic salt since there are various impurities such as fission products from spent nuclear fuels, dissolved ions from structural materials. Several compositions of electrolyte can be considered to analyze the influence of impurities on corrosion behavior of structural materials; LiCl-KCl eutectic salt (44wt% of LiCl, 99.99%, Sigma-Aldrich) containing lanthanides salts such as lanthanide chlorides ($LaCl_3$, 99.9%, Alfa Aesar) or rare earth chlorides (YCl_3, 99.95%, Alfa Aesar). As representative impurities, $LaCl_3$ was selected for cyclic voltammetry and YCl_3 for linear sweep voltammetry. To eliminate influence from moisture, the temperature of each salt was maintained at 200□ for 2 hours, then the salts were heated to target temperature of 773K-873K.

4.1.3 Reference electrode preparation

Fabrication of precise reference electrode is very important step for delicate electrochemical measurement in high temperature molten salts environment. There are some designs for fabrication of reference electrode for molten salt; one of them is Ag/AgCl electrode composed of an Ag wire, molten chloride salt with dissolved AgCl salt and an ion permeable membrane to prevent the direct transfer of solutions, but allow transfer of ions [13]. To meet these conditions, custom container tubes for reference electrode components were made using mullite with very thin bottom layer of less than 0.2mm. Ag wire (99.99%, Alfa Aesar) and LiCl-KCl eutectic salt containing 1wt% AgCl (99.99%, Alfa Aesar) were inserted in the mulite ceramic tube, then the tube was installed in the electrolyte carefully to prevent the damage at the bottom layer.

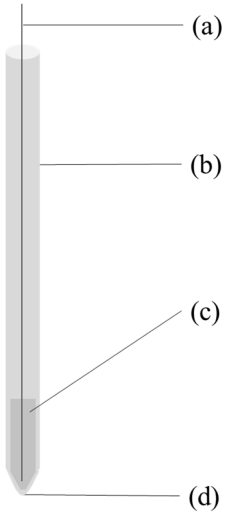

Fig. 6. Schematic diagram of Ag+/Ag reference electrode. (a) Ag wire, (b) Mullite tube, (c) LiCl-KCl with 1wt% of AgCl, (d) thin bottom tip

4.2 Experimental cell system for corrosion study

The experimental electrochemical cell was designed as 3 electrode system with a counter electrode made by twisted tungsten wire. To prevent shortcut of electrodes, working and counter electrodes were separated by quartz guide tube. As an electrolyte, 6 grams LiCl-KCl eutectic salt with selected impurities was contained in quartz test tube (Φ2*H500 mm). Thermocouple was applied in equivalent quartz test tube at similar position. During experiment argon atmosphere was maintained with the monitoring using oxygen sensor and moisture sensor. For whole corrosion experiment processes, O_2 and H_2O concentration were constrained below 4 ppm, 1 ppm respectively. The geometry of electrochemical cell and heating system are given in **Fig. 7**. Each electrode was connected with Versastat 3F potentiostat (Princeton Applied Research) to utilize electrochemical techniques for analysis of corrosion behavior.

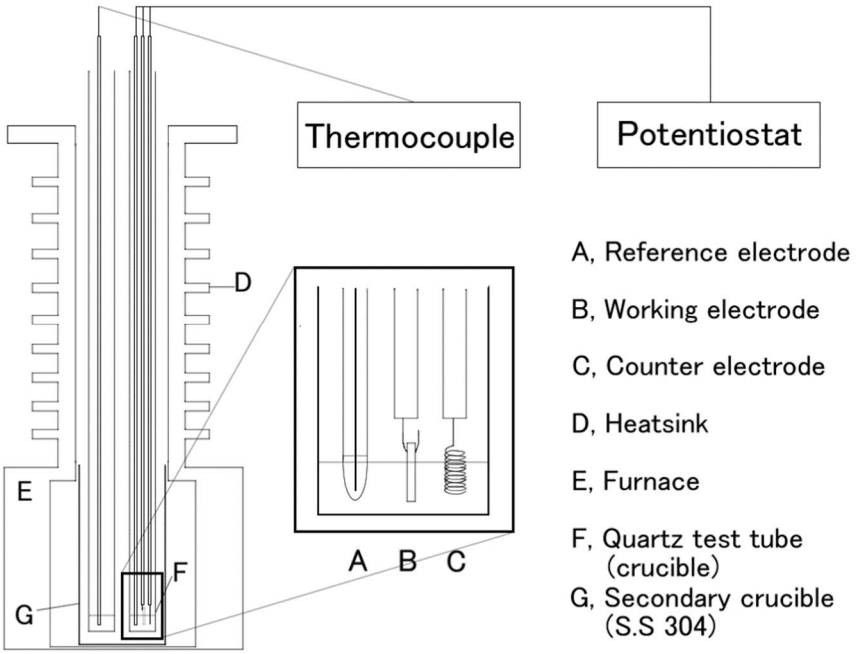

Fig. 7. Configuration of experimental cell and equipments Electrochemical techniques

Chloride molten salts are highly hygroscopic and easily react with oxygen in the air. In addition, the eutectic melting point of LiCl-KCl is 352°C and the actual process temperature is 773K, so this characteristic can be worse. Therefore, the work should be done in a controlled environment of water and oxygen concentrations. In order to conduct the electrochemical experiment of high temperature molten salt, a glove box environment which can keep oxygen and water below 1ppm is constructed as shown in **Fig. 8.**

Fig. 8. Globe box for controlled environment for electrochemical experiment

4.3 Electrochemical techniques

The cyclic voltammetry(CV) technique is an electrochemical technique that can specify and observe the concentration of a substance by analyzing the electrochemical characteristics of the substance in the electrolyte by observing the current changing through the cyclic voltage change. The CV test verifies the purity of the molten salt and verifies the performance of the reference electrode by identifying the redox peak of the material in the molten salt. In this experiment, $LaCl_3$ was adopted as a test substance to be added to the LiCl-KCl eutectic salt, and the reliability of the experimental environment was verified by comparing the redox potential and current density of La/La^{3+} with the reference case. Experiments were performed on 773K LiCl-KCl-5wt% LaCl3 molten salt, using a tungsten rod of 1mm diameter for WE and an Ag/AgCl electrode for reference electrode. After the cell was installed, it waited for at least 2 hours to electrochemically stabilize the interface between the molten salt and each electrode.

The linear sweep voltammetry(LSV) is a technique for measuring the electrochemical characteristics of samples or electrodes by changing the voltage at a constant rate with time to cause an oxidation or reduction reaction on electrode surface, and analyze the current generated in the process. In this study, LSV was used to measure the Tafel curve and polarization resistance of selected materials, and the corrosion resistance were tested over a maximum of 100 hours. Inconel 600 was measured every hour by measuring the polarizaton resistance and the tafel slope within ± 5 mV of the corrosion potential to measure the change of corrosion rate with time. The hourly measuring process is automated by program to minimize human error while each measuring. The algorithm is shown on **Fig.9**.

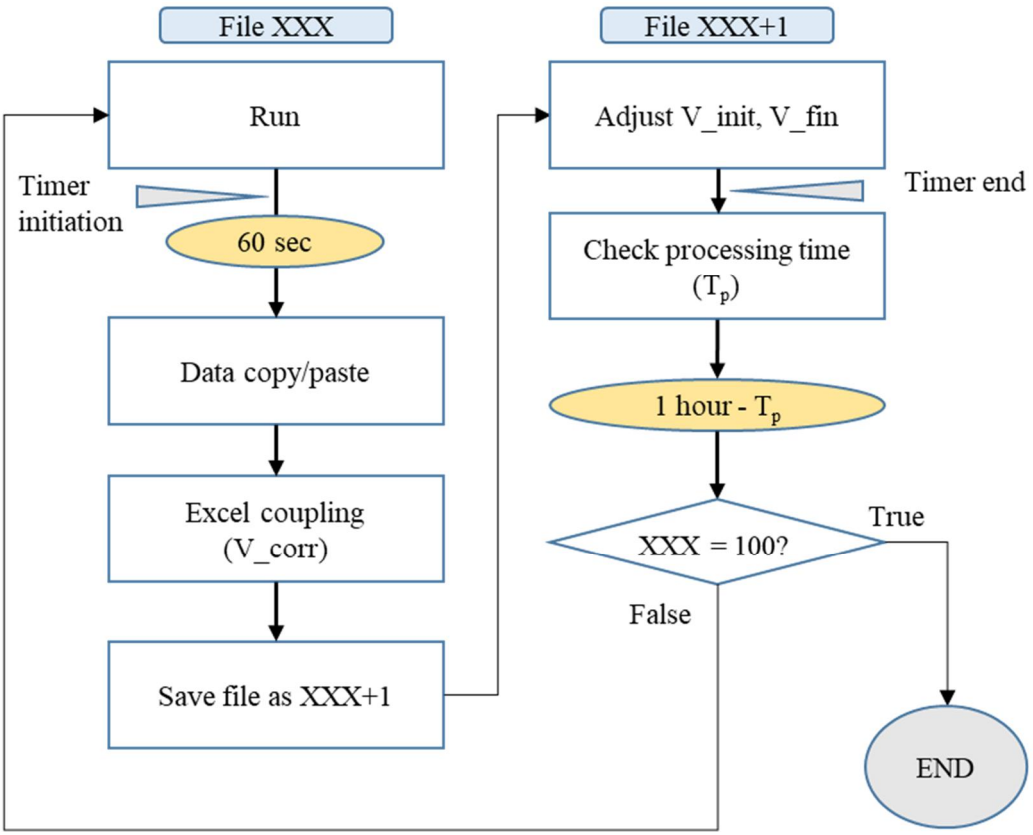

Fig. 9. Program algorithm automated for hourly electrochemical measurement built with python

Experimental raw data measured through LSV every hour have significant noise and are difficult to analyze as they are. In order to facilitate the analysis, the graph is smoothed by applying the robust local regression method which simulates the original data even in case of very severe noise in the two dimensional graph.

For robust local regression, at target point x_0, the number of k nearest data are gathered. The ratio $s = k/n$ of the collected data to the number of total data(n) is the span percentage.

Apply the weights of $K_{i0} = K(x_i, x_0)$ to the collected data by the distance from x_0, respectively. No weight is given if the data were more than five times far from the median. Then, weighted least squares regression is applied.

$$\sum_{i=1}^{n} K_{i0}(y_i - \beta_0 - \beta_1 x_i)^2$$

At this time, applying $\hat{\beta}_0$ and $\hat{\beta}_1$, which minimizes the value, the correction value $\hat{f}(x_0)$ at x_0 is

$$\hat{f}(x_0) = \hat{\beta}_0 + \hat{\beta}_1 x_0$$

Correction was performed by applying span value at 773K, which has severe noise, to 30%, and span value at 873K, which has relatively low noise, by using span value of 10%.

4.4 SEM-EDS Analysis on microstructure

Corroded specimens after experiments are preconditioned by Pt coating to get clear microscopic images by increasing conductivity, then Scanning Electron Microscopy (SEM) and Electron Diffraction Scanning (EDS) were conducted to observe the composition of specimen for surface and cross sectional analysis

4.5 Analysis method

The measurement of corrosion rate through electrochemical experiments is based on the measurement of the intensity of corrosion density and the polarization resistance. Corrosion current density is measured by galvanic cells and Tafel extrapolination or polarization resistance by the concept of current density by dividing the intensity of current uniformly distributed on the electrode surface by the area of the specimen.

$$i_{cor} = \frac{I_{cor}}{A},$$

where

$i_{cor} = \text{corrosion current density } (\text{uA/cm}^2)$,

$I_{cor} = \text{current } (\text{uA})$,

$A = \text{area of specimen } (\text{cm}^2)$

Equivalence weight(EW) is the mass of metal oxidized by the charge of 1 Faraday. The assumptions and formulas should be applied differently for pure metals and for alloys. The following equations are corrosion equivalents for alloys

$$\text{EW} = \frac{1}{\sum \frac{n_i f_i}{W_i}},$$

where

$n_i = \text{the mass fraction of the } i^{th} \text{ element in the alloy}$,

$W_i = \text{the atomic weight of the } i^{th} \text{ element in the alloy}$,

$n_i = \text{the valence of the } i^{th} \text{ element in the alloy}$

Corrosion current density is calculated from Stern-Geary coefficient

$$i_{corr} = 10^6 \frac{B}{R_p} \ (muA/cm^2)$$

where B is Stern-Geary coefficient,

$$B = \frac{b_a b_c}{2.303(b_a + b_c)} \ (V),$$

where

$b_{a(c)} =$ anodic(cathodic) Tafel slope.

Corrosion rate can be calculated in the froms of penetration rate (CR) or mass loss rate (MR)

$$CR = 3.27 \times 10^{-3} \frac{i_{cor} EW}{\rho} \ (mm/yr)$$

$$MR = 8.954 \times 10^{-3} i_{cor} EW \ (g/m^2 d)$$

Polarization resistance can be determined using potentiodynamic measurements at the corrosion potential or stepwise potentiostatic polarization at ± 5 or 10 mV. Potentiodynamic measurements can be used to derive the change in the slope of the current (I) - power (E) graph. Most electrochemical measurement devices use a slope of this graph as the polarization resistance by switching the current to current density. **Fig. 10.** shows the example of measuring polarization curve R_p.

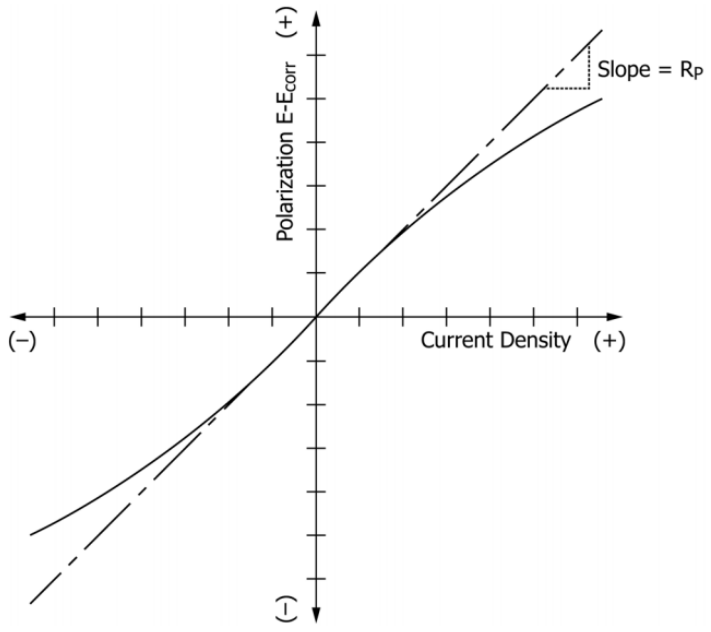

Fig. 10. Determination of polarization resistance R_p from short range of I-E curve.

V. Results & Discussions

5.1 Verification of Experimental Measurement System

Before the corrosion experiment, the comparison with the existing researches on the molten salt, and the experimental equipments was conducted except the specimens to verify the future measurement and analysis methods. As a measurement technique, the stability of the interfacial state of the electrode is checked through the open circuit test provided by the potentiometer Versastat 3F and the accompanying software Versastudio. The multiple cyclic voltammetry is used to identify the oxidation and reduction phenomenon at a specific voltage, the reliability of reference electrode and the ability to detect impurities were evaluated. The following is the result of multiple cyclic voltammetry measurement of LiCl-53.2wt% KCl-5wt% $LaCl_3$ at 773K and comparison with the reference case. The measurement range is [-2.5V, 0V] and [-2.3V, 0.5V], the scanning rate is 300mV, and 5 cycles are performed and the second cycle is choosed for comparison. A tungsten wire was used as a working electrode and a counter electrode, and an Ag/AgCl electrode was used as a reference electrode. The diameter of the electrode is 1 mm. Measurements were performed after 1 hour from the insertion of the electrode for interfacial stability.

Fig. 11.(a) shows the result of cyclic voltammetry test and reference CV curve. During the process, La^+/La and Li^+/Li reduction occurs at -2.0V and -2.25V. The result shows that reference electrode potential is approximately similar with **Fig. 11.(c),** the reference case. Since there is difference on reference electrode and the amount of LaCl3 is 5 times more than reference case, the shape of peak and current are not exactly matched.

To compare CV curve with reference case quantitatively, considering the difference on reference electrode, then **Fig. 11.(b)** what the range is [-2.3V, 0.5V] would be compared with **Fig. 11.(d)**. The reference Ag/AgCl electrode used on reference case is Ag/0.1 mol% AgCl in LiCl-KCl in pyrex, but the reference electrode used by this study is Ag/1wt% AgCl, or Ag/0.3924 mol% AgCl in mullite. Assuming that the difference yielded by membrane material is negligible, different Nernst equilibrium potential make the difference between two reference electrodes. The Nernst equation at 773K for Ag/Ag^+ is

$$E = E^{\circ} - 0.1536 \ \ln(\frac{a_{red}}{a_{ox}})$$

Therefore, the difference in equilibrium potential to reference case is -0.0912V, about -0.1V. Therefore, it is reasonable that the potentials at redox peaks of (b) is lower than (d) for about -0.1V.

The current density should be considered in order to compare peak current quantitatively. The area of apparent electrode is 0.347 cm^2 for reference case and 0.471 cm^2 for this study. Assuming that the ratio

of LaCl3, LiCl and KCl is maintained at 773K, then the concentration of $LaCl_3$ of this study is about 4.22×10^{-4} mol cm^{-3}, which is 5.59 times bigger than reference case (7.54×10^{-5} mol cm^{-3}). Cathodic peak current density of this study and the reference case (250mV/sec) are about -0.531 A/cm^2 and -0.0865 A/cm^2, respectively. Scan rate of this study and the reference case are 300mV/sec and 250mV/sec, respectively. The difference of diffusion coefficient is assumed to be negligible.

According to Randles – Servick equation, the cathodic or anodic peak current is

$$\mathrm{i_p} = 0.4463nFAC\left(\frac{nFvD}{RT}\right)^{0.5}$$

From this relation and assumption, the ratio of calculated $LaCl_3$ concentration of this study(C_0) and reference case(C_1) is

$$\mathrm{C_0}: C_1 = \frac{i_0}{A_0 v_0^{0.5}} : \frac{i_1}{A_1 v_1^{0.5}} = 5.60:1$$

The calculated concentration ratio from Randles – Servick equation is very similar with actual ratio of 5.59, so the experimental cell well matches with reference data.

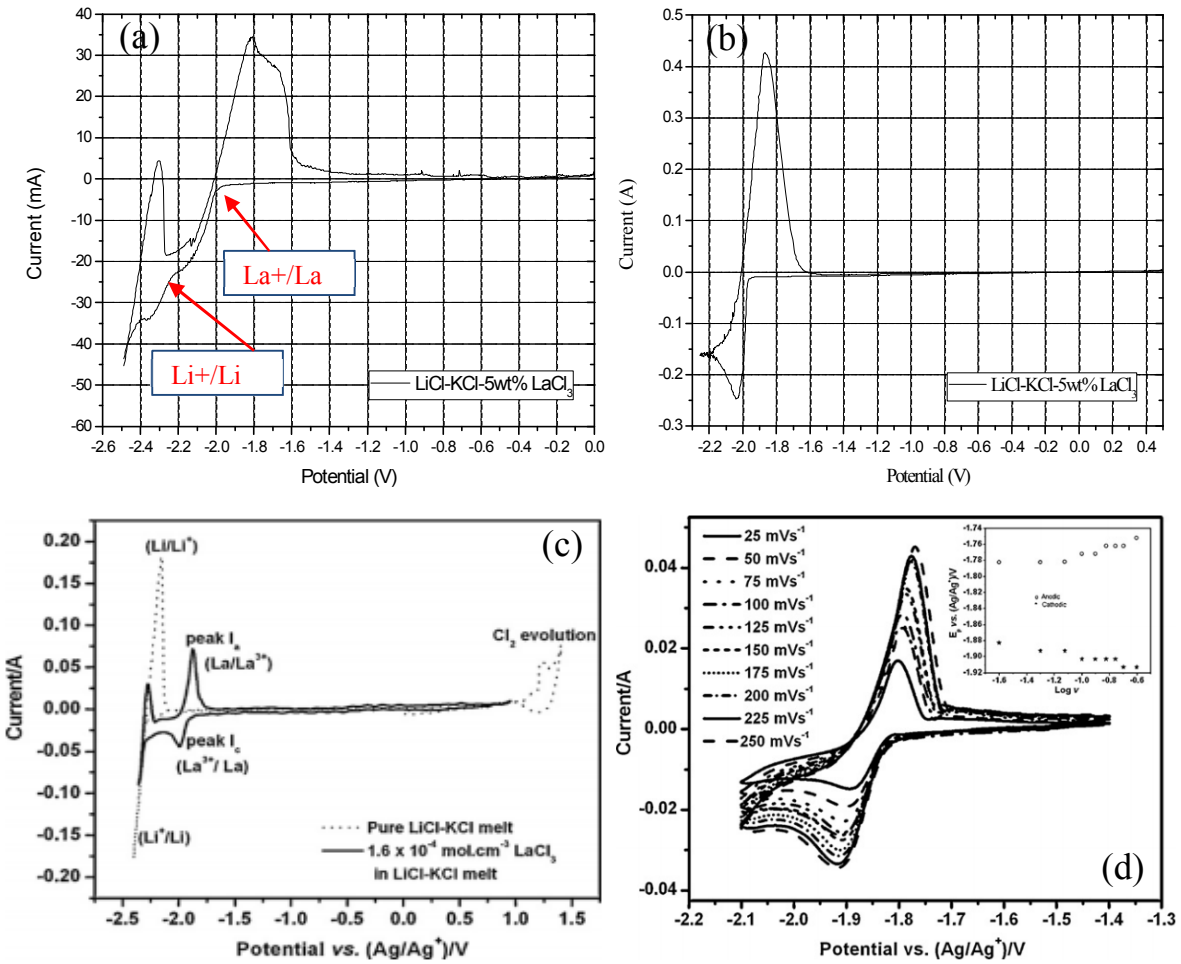

Fig. 11. Cyclic voltammograms for test cell on (a) [-2.5V, 0V], (b) [-2.3V, 0.5V] and reference voltammograms for (c) both La^{+}/La and Li^{+}/Li and (d) only La^{+}/La. Working electrode is tungsten. Electrolytes are LiCl-KCl- 4.22×10^{-4} $LaCl_3$ for (a) and (b) and LiCl-KCl- 7.54×10^{-4} $LaCl_3$ for (c) and (d). Cell temperature is 773K.

5.2 Electrochemical measurement of corrosion behavior

Inconel 600, which is considered as a suitable structural material of electrorefiner, was subjected to more practical corrosion experiments. **Fig. 12** summarize the results of the corrosion current measured for 100 hours in the temperature range of 773 ~ 873K by using YCl_3 as an impurity in the LiCl-KCl eutectic salt environment.

Since the design of the electrolytic refining bath of the actual pyro-processing will be an environment with a temperature of 773K and various impurities added, the (A) environment is most similar to that of the actual electrorefiners among the three measured environments. The (B) and (C) environments were tested at higher temperatures than the (A) environment, thus accelerating the corrosion phenomenon through harsher environments and trying to understand the time-dependent effects more densely.

The result of (A) shows significant local deviations over the whole measurement time, but the overall current density level is 40 uA/cm^2 and the measurement time is limited to 100 hours, which seems insufficient to understand the behavior of the corrosion rate over time. In order to understand the initial corrosion behavior and the corrosion behavior when it is finally stabilized, it is expected that the measurement should continue more after 100 hours.

In the case of the result B, the local deviation is relatively small compared to the case of A or (C), but the variation with time rises suddenly in the interval of 0~15 h and the interval of 56~75 h. Particularly, the behavior in the initial time interval is similar to that in the case (C), but since the case (C) has a very large initial current density, it is hard to say that the same mechanism works on both cases. In case B, the corrosion current density is in the range of 10~20 uA/cm^2 at 15~56 h, and gradually decreases and stabilized to about 70 uA/cm^2 until 80h. In particular, it is supposed that a certain corrosion mechanism occurred between 15 and 56 h, and then returned to the initial corrosion mechanism since it was fixed at a current density similar to the current density level before 5 h. However, it is not known whether the corrosion current density will continue as stabilized after 100 hours, so additional measurement is recommended.

The environment of (C) shows a very high corrosion current density in the early part of the measurement, but the corrosion current density goes down to similar level of the measurement results in other environments up to about 25 h. The corrosion current density is relatively low at 30 h, about 15uA/cm^2, but then gradually increased at almost linearly, more than doubling to about 35 uA/cm^2 at 100h. At around 58h, the deep which shows a drastic decrease in the corrosion current density is seen, but it seems to be a measurement error since it returns to the original trend soon. There is also a high local deviation similar to Case (A). It is predicted that the corrosion behavior after 100 h is easy to predict compared with the measurement results of other cases that the corrosion current density will be continuously increased for a considerable time based on the linear increase pattern. However, longer

measurement seems to be required for more accurate study.

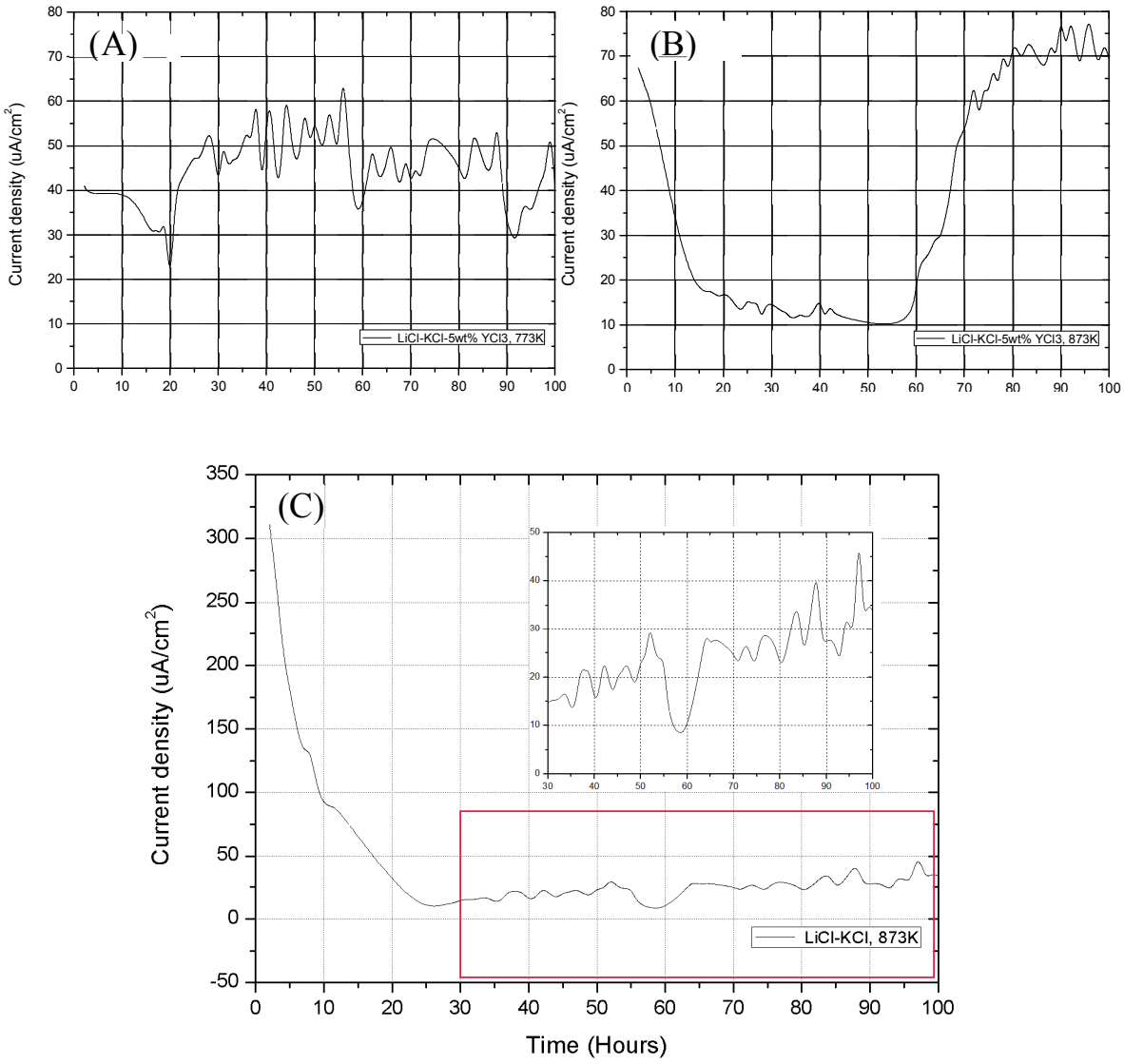

Fig. 12. Hourly Corrosion current density of (A) LiCl-KCl-5wt% YCl3, 773K, (B) LiCl-KCl-5wt% YCl3, 873K and (C) LiCl-KCl, 873K for 100 hours. (cont')

The corrosion rate was calculated for each case by using the measured corrosion current density as shown in **Fig. 13**, and the corrosion behavior was analyzed by combining with the change of corrosion potential. The corrosion rate is calculated by applying the material properties of the specimen to the corrosion current density, as shown in the ASTM Guidelines, so that it basically appears as the behavior of the corrosion current density.

Case (A) also exhibits significant deviations in corrosion potential as shown by relatively high corrosion rate deviations. The corrosion potentials converge about 128 mV vs Ag/AgCl after 30 hours. The corrosion rate is about 0.45 mm/yr at 100 h.

Case (B) shows a tendency for corrosion potential to decrease continuously until 46 hours. Especially, in the interval up to 15 h, corrosion potential decrease much steeply, and the corrosion rate is rapidly falling in that interval. The corrosion rate also drastically increases from about 0.1 mm/yr to 0.6 mm / yr from 46 h where the corrosion potential becomes less variable around -145 mV to 70 h at -150 mV. If the surface of the specimen during the relevant time period is analyzed and it is possible to ascertain which factors cause the rapid deterioration of the corrosion rate, this factor could be used as an important clue to improve the corrosion resistance of the electrolytic refining furnace.

Case (C) shows drastic drops of the corrosion potential from about 140 mV to -15 mV from the initial 25 hours. In this process, the corrosion rate also drops rapidly from the very high level of more than 3.3 mm/yr to a low level of 0.25 mm/yr, so there seems to be a very weak component of the initial corrosion of the surface of the specimen. After 25 hours, the corrosion potential is maintained at a relatively high level of -45 to -30 mV, and the corrosion rate is gradually increased from 0.25 mm/yr at 25 h to 0.34 mm / yr at 100 h. Among the three experiments up to 100 h, the relative corrosion rates were lowest in case (C).

The corrosion potential and corrosion rate after 100 hours of corrosion test for each case are shown in **Table 7**. The lower the corrosion potential, the greater the tendency of the specimen to be oxidized and the faster the corrosion occurred. The corrosion potentials of the three cases were generally in the order of C > A > B, which is the reverse order of the corrosion rates. However, the initial corrosion behavior of (B) and (C) cases (873K) showed that the corrosion rate was also higher at the point where initially the corrosion potential was gradually lowered. It is reasonable to assume that the composition of the molten salt rapidly dissolves in the early stage of corrosion until a certain percentage of the metal chloride from the specimen is reached, rather than said that the change of material composition of the specimen surface leads the rapid corrosion.

The temperature shows a positive correlation with the corrosion rate. Case (A) and Case (B) differed only in temperature, and the corrosion rate at 100 h was 0.41579 mm/yr for (A) and 0.70466 mm/yr for B. At 873K, the corrosion rate was about 70% faster than at 773K.

Impacts of impurities on the rate of corrosion seem to be very negative for corrosion characteristics, although more measurements and analysis are required. Case (B) with impurity YCl_3 was more than twice as fast as case (C). Even case (A) with a temperature of 773K was about 21% higher in corrosion rate than the 873K case with no impurities. The cause could be the difference in Gibb's free energy shown in **Table 2**. The Gibb's free energy of YCl_3 is higher than that of the LiCl-KCl eutectic salt at a temperature of 873K, but lower than that of the chloride compounds of the Inconel 600 Components. Therefore, YCl_3 may accelerate corrosion by becoming a stepping-stone for chloride formation of Cr, Fe, Ni of Inconel 600, or yttrium may form yttrium compound with other metal components on the surface of the Inconel 600.

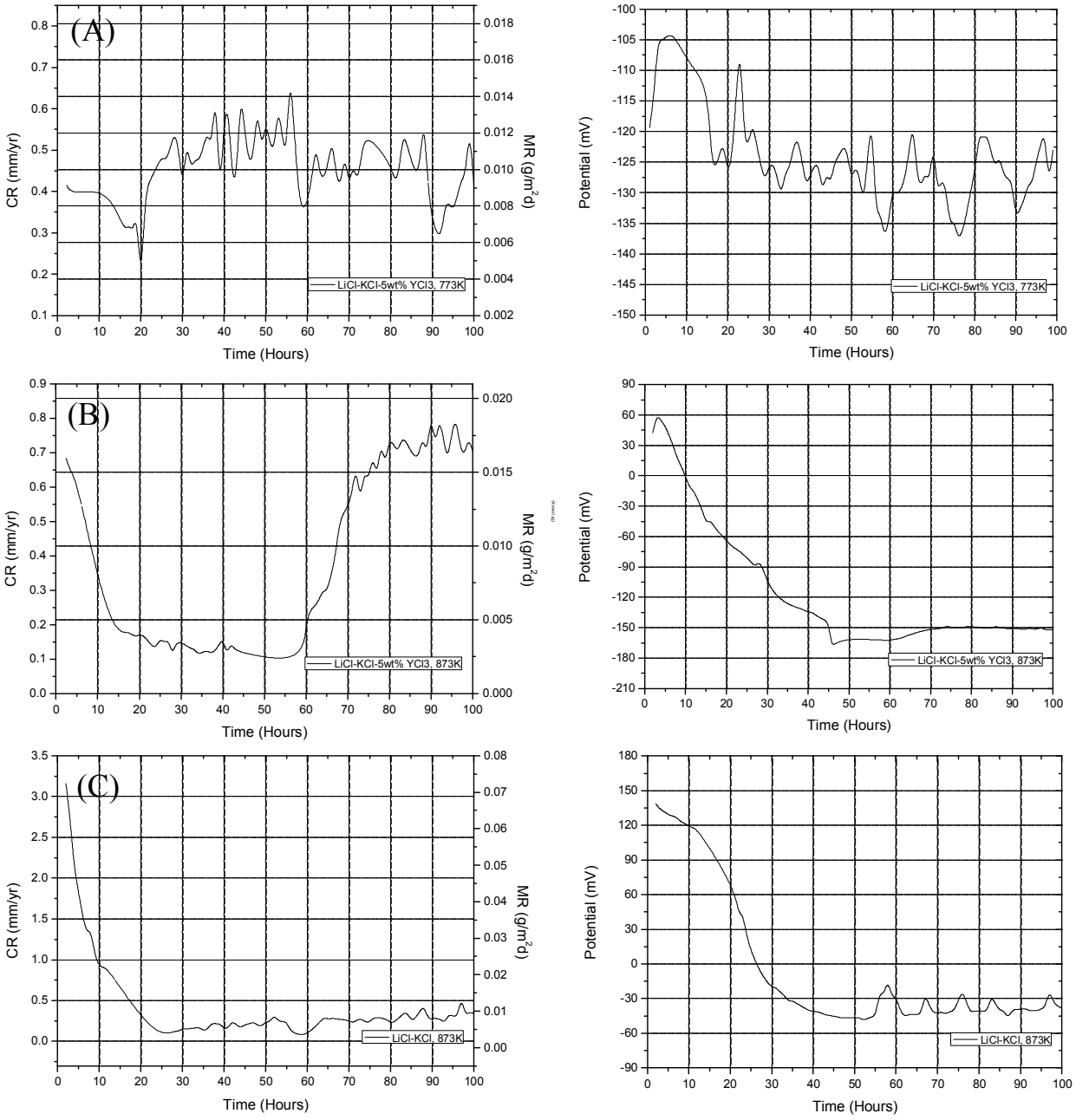

Fig. 13. Corrosion rate and corrosion potential for (A) LiCl-KCl-5wt% YCl3, 773K, (B) LiCl-KCl-5wt% YCl3, 873K and (C) LiCl-KCl, 873K for 100 hours**.**

Table 7. Corrosion rate and corrosion potential of each experimental cases at 100 hours.

Experiment	Corrosion rate (mm/yr, 100 h)	Corrosion potential (mV)
A	**0.41579**	**-123**
B	**0.70466**	**-152**
C	**0.34357**	**-38**

5.3 SEM-EDAX microscopic analysis

To better understand the mechanism by which impurities affect the rate of corrosion, the surface of the specimen after 100 h corrosion test was cleaned and measured by SEM-EDAX techniques to be analyzed. **Fig. 14** is the surface SEM image of Inconel 600 after corrosion test in 873K LiCl-KCl-5 wt% YCl3 molten salt and the result of EDAX analysis of composition ratio of the components. As a result, there were no yttrium compound remained on the surface, and the content of Cr was drastically decreased from 15.48 wt% to 12.21 wt%. The reason is that Gibbs free energy of $CrCl_3$ (-60.4 kJ/mol Cl_2) is higher than $NiCl_2$ (-45.7 kJ/mol Cl_2) and $FeCl_3$ (-58.8 kJ/mol Cl_2).

The relative contents of Fe and Ni are shown in **Fig. 15** except for Cr which shows a large change. Ni has leached out at a similar rate from that of Fe despite low Gibb's free energy because the content of Ni is more than 10 times higher than that of Fe, so the surface area where the electrochemical reaction occurs is much larger.

Cross-sectional SEM-EDAX was performed to understand the composition change due to the corrosion penetration. **Fig. 16** is the SEM-EDAX results of the Inconel 600 specimen which was subjected to the corrosion test for 100 hours in the 873K molten salt of LiCl-KCl with or without impurities. **Fig. 16.1** and **2** have a high content of C on the surface, but this is probably the residue of carbon tape to hold the specimen. **Fig. 16.3** and **Fig. 16.4** was experimented in a harsh environment compared to **Fig. 16.1** and **Fig. 16.2**, but no change in composition was observed on the surface. It seems that it is difficult to grasp the corrosion characteristics about corrosion penetration through the 100 hours' corrosion test.

Before corrosion, Inconel 600, 873K

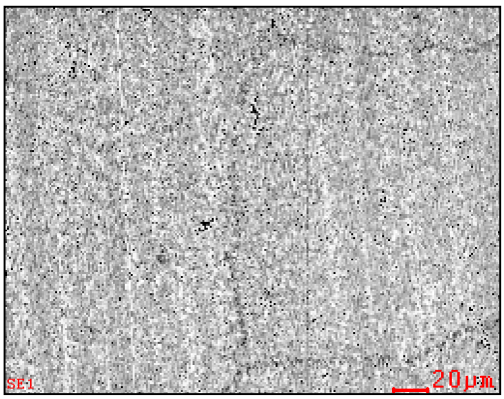

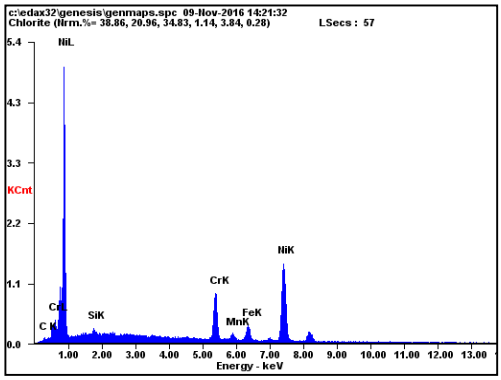

Element	Wt%	At%
Ni	75.50	70.84
Cr	15.48	16.40
Fe	7.31	7.21
Mn	0.13	0.13
Si	0.68	1.33
C	0.89	4.08

After corrosion, Inconel 600, 873K

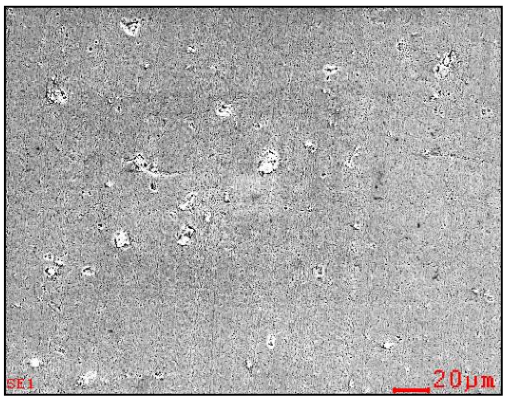

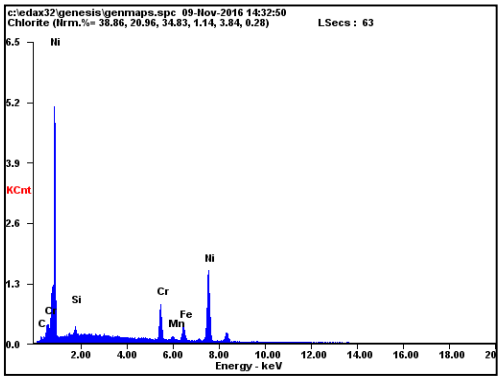

Element	Wt%	At%
Ni	77.19	70.31
Cr	12.21	12.55
Fe	7.51	7.19
Mn	0.37	0.36
Si	0.99	1.89
C	1.73	7.78

Fig. 14. SEM microphotograph and EDAX composition map for Inconel 600, tested in LiCl-KCl eutectic salt at 873K for 100 hours.

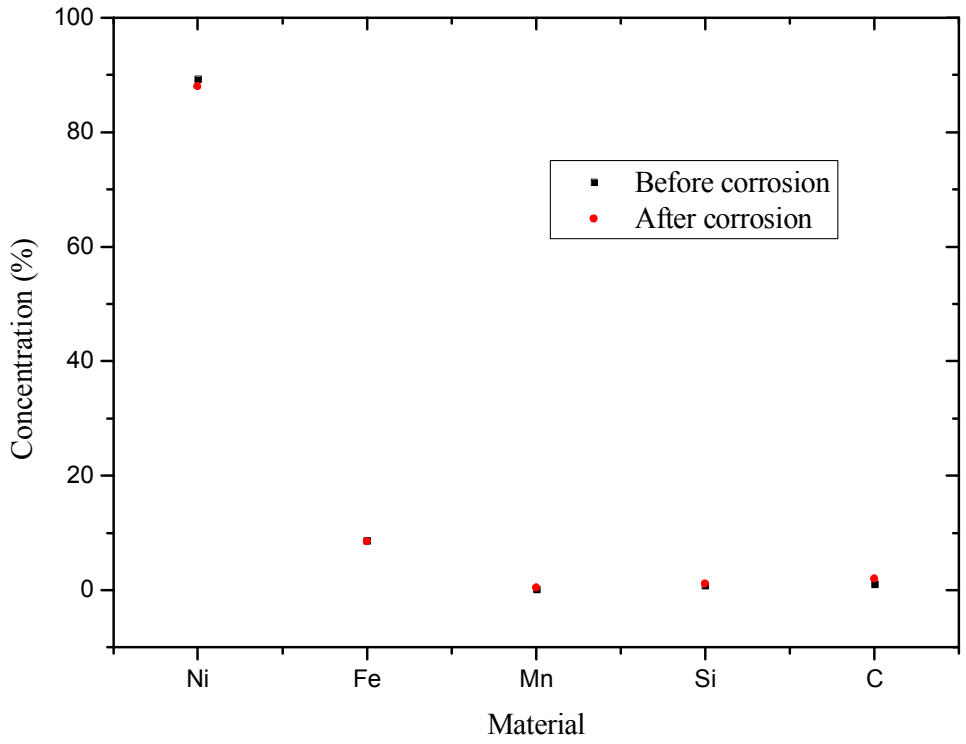

Fig. 15. Relative concentration of composition materials without Cr of the result from EDAX on Inconel 600 tested in LiCl-KCl at 873K for 100 hours.

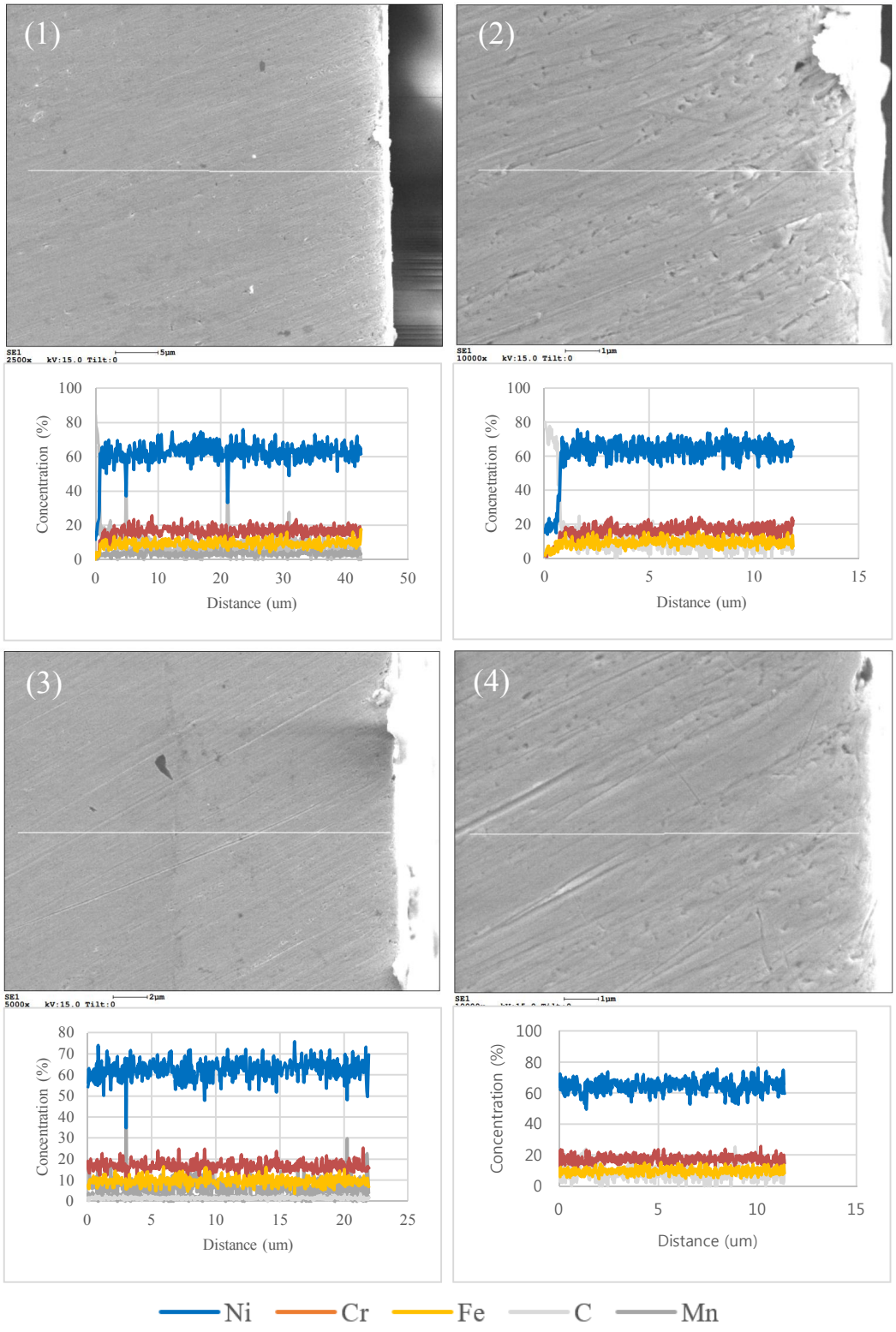

Fig. 16. SEM-EDAX Line composition distribution of LiCl-KCl for x2500(1,3) and x10000(2,4) Microphotograph of Inconel 600 tested in LiCl-KCl (1,2) and LiCl-KCl-YCl_3 (3,4) at 873K.

VI. Conclusions

Since LiCl-KCl eutectic molten salt is a main electrolyte used for electrorefining and electrowinning of pyroprocessing, it is very important to study the corrosion characteristics simulating the actual operating environment of the structural material. In this paper, the corrosion behavior of structural materials in the LiCl-KCl eutectic salt environment containing Yttrium chloride as an impurity was measured at actual operating temperature, 773K, and more severe condition, 873K for 100 hours to study initial corrosion behavior. The experimental cell was designed to prevent the evaporation of molten salt and keep the electrochemical environment uniform throughout the experiment. Polarization resistance method was applied to minimize the damage on the specimen and to carry out precise measurement every hour by automated measurement.

In the eutectic mixed salt environment of 773K and 873K the corrosion potential, the corrosion current density and the corrosion rate of Inconel 600 were measured by the presence or absence of impurities. The initial corrosion behavior was analyzed in relation to corrosion potential and corrosion rate. It was experimentally identified that YCl_3, the rare earth impurity had a significant negative impact on the corrosion characteristics of Inconel 600 in the LiCl-KCl environment, and the effect of corrosion on up to 100 hours was quantitatively evaluated. In addition, SEM-EDAX analysis were used to investigate the compositional changes in the surface and cross-sectional area of the specimens, which were correlated with Gibb's free energy.

In reality, impurities are inevitably accumulated in the molten salt electrolytes as the actual pyrolysis process proceeds. Since it has been identified that the impurities affect the corrosion rate of the pyroprocessing structural material, it is necessary to study the molten salt environment in which various impurities are added. In addition, since the hourly analysis of corrosion characteristics performed in this study depends on only electrochemical techniques and data, the basis is insufficient, so it is necessary to perform deep component analysis with more techniques for various time intervals. Finally, Since the corrosion rate has not fully converged within 100 hours, a longer period of corrosion testing needs to be performed to determine practical corrosion behavior for actual pyroprocessing operations.

REFERENCES

[1] Radioactive Waste in Perspective, p74, IAEA/NEA, 2010

[2] G. Volckaert et al., "National Inventories and Management Strategies for Spent Nuclear Fuel and Radioactive Waste. Methodology for Common Presentation of Data," 2016.

[3] Korean Ministry of Trade, Industry and Energy, 2018

[4] Nuclear Energy Agency and Organisation for Economic Co-operation and Development, "Spent nuclear fuel reprocessing flowsheet," Nea/Nsc/Wpfc/Doc(2012)15, no. June, p. 120, 2012.

[5] M. S. Manohar S. Sohal, M. A. Matthias A. Ebner, and P. Piyush Sabhar, "Engineering Database of Liquid Salt Thermophysical," no. June, 2013.

[6] D. R. Stull and H. Prophet, JANAF Thermochemical Tables, NSRDS-NBS 37, U.S. Dept of Commerce, National Bureau of Standards, 1971

[7] "Standard Gibb' s Energies of Formation for," J. Soc. Chem. Ind.(London), vol. 63, no. 125, 1944.

[8] N. S. Patel, V. Pavlík, and M. Boča, "High-Temperature Corrosion Behavior of Superalloys in Molten Salts–A Review," Crit. Rev. Solid State Mater. Sci., vol. 42, no. 1, pp. 83–97, 2017.

[9] K. Vignarooban, P. Pugazhendhi, C. Tucker, D. Gervasio, and A. M. Kannan, "Corrosion resistance of Hastelloys in molten metal-chloride heat-transfer fluids for concentrating solar power applications," Sol. Energy, vol. 103, pp. 62–69, 2014.

[10] M. Hofmeister, L. Klein, H. Miran, R. Rettig, S. Virtanen, and R. F. Singer, "Corrosion behaviour of stainless steels and a single crystal superalloy in a ternary LiCl-KCl-CsCl molten salt," Corros. Sci., vol. 90, pp. 46–53, 2015.

[11] A. Ravi Shankar, K. Thyagarajan, and U. Kamachi Mudali, "Corrosion behavior of candidate materials in molten LiCl-KCl salt under argon atmosphere," Corrosion, vol. 69, no. 7, pp. 655–665, 2013.

[12] J. I. Barraza-Fierro, M. A. Espinosa-Medina, M. Hernandez-Hernandez, H. B. Liu, and E. Sosa-Hernandez, "Effect of Li and Cu addition on corrosion of Fe-40at.% Al intermetallics in molten LiCl-KCl eutectic salt," Corros. Sci., vol. 59, pp. 119–126, 2012.

[13] L. Yang and R. G. Hudson, "Some Investigations of the Ag/AgCl in LiCl-KCl Eutectic Reference Electrode," J. Electrochem. Soc., vol. 106, no. 11, p. 986, 1959.